Research Article

Maha Abdallah Alnuwaiser, Mohamed Rabia*, Asmaa M. Elsayed

Magnetite–poly-1*H* pyrrole dendritic nanocomposite seeded on poly-1*H* pyrrole: A promising photocathode for green hydrogen generation from sanitation water without using external sacrificing agent

https://doi.org/10.1515/chem-2024-0106
received August 16, 2024; accepted October 6, 2024

Abstract: The Fe_3O_4 magnetite–poly-1*H* pyrrole dendritic nanocomposite seeded on additional poly-1*H* pyrrole film, denoted as Fe_3O_4-P1HP/P1HP, is synthesized by oxidative polymerization utilizing $(Fe(NO_3)_3{\cdot}5H_2O$ for the pyrrole monomer. The resulting nanocomposite exhibits a notable bandgap of 1.97 eV and demonstrates broad optical absorption up to 625 nm. The structure of each particle consists of numerous smaller internal particles, which are composed of nanofibers of approximately 2.0 nm in length and porous structures of around 5.0 nm. These porous structures cluster together to form a larger configuration, with an overall diameter of ~230 nm and a length of approximately 300 nm, giving the composite a nano-cactus-like appearance. The fabricated Fe_3O_4–P1HP/P1HP photocathode is inserted into a three-electrode cell to facilitate green hydrogen production from sanitation water without the need for any external sacrificial agent. The performance of H_2 gas generation is assessed by measuring the photocurrent density (J_{ph}) under light, which serves as an indicator of the efficiency of hydrogen production. The J_{ph} value reaches −0.23 mA/cm² under light conditions. The highest J_{ph} values of −0.164 and −0.158 mA/cm² are observed at wavelengths of 340 and 440 nm, respectively. However, as the wavelength reaches 540 nm, the J_{ph} value decreases to −0.134 mA/cm² and drops to its lowest point of −0.128 mA/cm² at 730 nm, which is comparable to the dark current (J_o). The fabricated photocathode demonstrates a promising hydrogen generation rate of 90 μmol/h cm², reflecting its potential for commercial applications. The combination of this impressive hydrogen production rate, along with the photocathode's cost-effectiveness and straightforward fabrication process, suggests that this technology could be commercially viable for converting sanitation water into hydrogen gas.

Keywords: poly(1*H* pyrrole), Fe_3O_4, photocathode, hydrogen generation, sanitation water

1 Introduction

The pursuit of renewable energy sources that are both cost-effective and efficient represents a significant challenge for researchers today. This challenge is driven by the need to create solutions that not only provide sustainable energy but also contribute to an eco-friendly and green chemistry environment [1–3]. By advancing renewable energy technologies, researchers aim to lessen our reliance on fossil fuels, which have become increasingly problematic in recent years due to their detrimental effects on the environment. Fossil fuels, once the cornerstone of global energy production, have now become a focal point of concern due to their association with pollution, climate change, and other environmental issues. The extraction, processing, and burning of these fuels release harmful greenhouse gases and other pollutants into the atmosphere, contributing to global warming and environmental degradation. As a result, the urgent need to shift towards renewable energy sources has become a priority for the scientific community. Renewable energy sources such as solar,

* **Corresponding author: Mohamed Rabia**, Nanomaterials Science Research Laboratory, Chemistry Department, Faculty of Science, Beni-Suef University, Beni-Suef, 62514, Egypt,
e-mail: mohamedchem@science.bsu.edu.eg
Maha Abdallah Alnuwaiser: Department of Chemistry, College of Science, Princess Nourah bint Abdulrahman University, P.O. Box 84428, Riyadh, 11671, Saudi Arabia, e-mail: maalnoussier@pnu.edu.sa
Asmaa M. Elsayed: TH-PPM Group, Physics Department, Faculty of Science, Beni-Suef University, Beni-Suef, 62514, Egypt,
e-mail: asmaa.elsayed@science.bsu.edu.eg

wind, hydro, and bioenergy offer the promise of a cleaner, more sustainable future. However, the transition to these energy sources is not without its challenges. One of the primary obstacles is the cost associated with developing and implementing these technologies on a large scale. Researchers are tasked with finding ways to make renewable energy more affordable and accessible without compromising on efficiency and effectiveness [2,4].

Hydrogen is recognized as a clean fuel of the future, primarily because it produces zero carbon emissions, which positions sustainable H_2 generation as a crucial priority in the energy sector. Among the numerous technologies available for H_2 production, photoelectrochemical (PEC) technology stands out due to its innovative approach to water splitting. This method involves the use of various materials with photoresponsive properties, which harness light energy to drive the chemical reactions needed for hydrogen production. The process is enhanced by the presence of additional electrolytes in the reaction medium, which play a critical role in facilitating the movement of ions. These electrolytes ensure that the necessary charge transfer occurs efficiently, supporting the overall reaction process. The use of PEC technology in hydrogen production offers a promising pathway toward sustainable energy, as it leverages abundant solar energy and water, both of which are renewable resources. However, achieving high efficiency in this process requires the careful selection and optimization of materials with suitable photoresponsive properties. These materials must not only effectively absorb sunlight but also exhibit the necessary chemical stability and catalytic activity to drive the water-splitting reaction over extended periods. Through the advancement of PEC technology and the improvement of materials utilized in this process, researchers are working toward establishing a dependable and sustainable method for large-scale hydrogen generation. This strategy supports the larger objective of decreasing reliance on fossil fuels and minimizing the environmental effects of energy production, ultimately aiding the transition to a cleaner and more sustainable energy future [3,5,6].

Among various photocatalytic metal oxides studied, Wang et al. [7] demonstrated that CuO nanowires are beneficial for light detection in the IR domain. However, they observed a small photocurrent (20 μA) under high application conditions. In addition, ferric oxide has gained particular interest due to its relative abundance, non-toxicity, and affordability. Recent studies have highlighted the potential of nanoscale ferric oxides [8]. Fe_3O_4 is particularly notable for its advantageous properties, such as a 2.1 eV band gap [9], non-toxicity, low cost, and strong chemical stability in aqueous solutions. Furthermore, Fe_3O_4 has various uses in industries, including cement production, water splitting, gas detection, solar energy conversion, lithium-ion battery manufacturing, water purification, and pigmentation. These versatile uses have led to increased interest in the production of iron oxide nanoparticles for these fields [10].

The efficiency of Fe_3O_4 (magnetite) in hydrogen (H_2) production can be significantly enhanced by forming composites with other materials. The synergistic interactions between these combined materials are particularly promising, as they can generate hot electrons that actively engage in the reaction with nearby solutions, thereby boosting hydrogen production [11,12]. Additionally, the direct interaction between the morphology and optical properties of the composite materials plays a crucial role in this process. Porous nanomaterials are especially well suited for such photocatalytic applications due to their unique structure, which offers a high surface area and excellent light absorption capabilities. These characteristics allow for better light harvesting and more efficient charge separation, which are essential for maximizing the photocatalytic activity of Fe_3O_4 composites.

Conducting polymers has some achievements in this area, in which the tunable photophysical properties of P1HP, such as its photothermal conversion ability and Fenton catalysis ability, also enable emerging applications in cancer therapy, including tumor ablation and immune activation [13]. Despite previous studies significantly enhancing materials for H_2 gas generation, several challenges remain. These include issues such as limited production yield, the need for advanced preparation techniques, and the use of highly acidic or basic electrolytes, which can cause rapid and severe corrosion of the electrodes used for H_2 gas generation [14,15]. Therefore, it is essential to explore other technologies and conduct further studies to address these technical challenges.

Herein, the Fe_3O_4-P1HP/P1HP photocathode has been meticulously fabricated and thoroughly analyzed to assess its morphology, chemical composition, electrical properties, and optical behavior. This photocathode has demonstrated exceptional performance in hydrogen gas generation, as evidenced by the J_{ph} measurements conducted under both general light conditions and various monochromatic light exposures. The study also includes an evaluation of chopped light, which highlights the sensitivity and reproducibility of the fabricated photocathode.

The hydrogen gas production rate was calculated using sanitation water as the electrolyte, notably without the addition of any external sacrificial agents. The Fe_3O_4-P1HP/P1HP photocathode stands out for its efficient hydrogen generation capabilities coupled with cost-effectiveness, positioning it as a promising material. Its unique structural characteristics and robust performance under light conditions indicate that this technology could significantly contribute to sustainable energy solutions, particularly in converting

sanitation water into hydrogen gas. The potential for scaling and industrial implementation further enhances the photocathode's appeal, suggesting that the Fe_3O_4-P1HP/P1HP photocathode could have great behavior in the future of green hydrogen production. As a valuable advancement in this field, it combines innovative design with practical advantages, offering a pathway toward more sustainable and economically viable hydrogen generation processes.

2 Materials and methods

2.1 Materials and characterization techniques

The following chemicals were used in this study: ferric nitrate pentahydrate ($Fe(NO_3)_3{\cdot}5H_2O$, 99.9%, Pio-Chem Co, Egypt), ammonium persulfate $(NH_4)_2S_2O_8{\cdot}5H_2O$, 99.9%, Pio-Chem Co, Egypt), pyrrole (Across Co., 99.9%, USA), and HCl (36%, Merck, Germany). The sanitation water is supported by the company water (Beni-Suef city, Egypt, thrice treated).

Characterization techniques involved the use of various instruments for chemical analysis. These include the AXIS-NOVA for XPS, the Bruker for FTIR, and the Pro for XRD. To observe 3D and 2D morphologies, Zeiss and Jole devices were utilized for SEM and TEM, respectively. Optical properties were assessed using an Elmer Perkin device.

2.2 Fabrication of Fe_3O_4-P1HP/P1HP photocathode

The fabrication of the Fe_3O_4-P1HP/P1HP photocathode involves two key steps. Initially, a P1HP seeding layer is created on a glass substrate. This P1HP layer is formed by oxidizing pyrrole using $(NH_4)_2S_2O_8$ in an acidic medium, with the monomer, oxidant, and acid mixed in a ratio of 1:2.5:10. In the subsequent step, the Fe_3O_4-P1HP layer is deposited using a similar oxidation process, but this time with the inclusion of both $(NH_4)_2S_2O_8$ and iron nitrate nonahydrate $(Fe(NO_3)_3{\cdot}5H_2O$ maintaining the same ratio. These reagents not only facilitate the oxidation of pyrrole but also contribute to the formation of the Fe_3O_4-P1HP composite. The reaction is carried out in an acidic medium (0.5 M HCl), which significantly improves the morphology of the resulting polymer composite. Figure 1 shows an illustration of the deposition conditions.

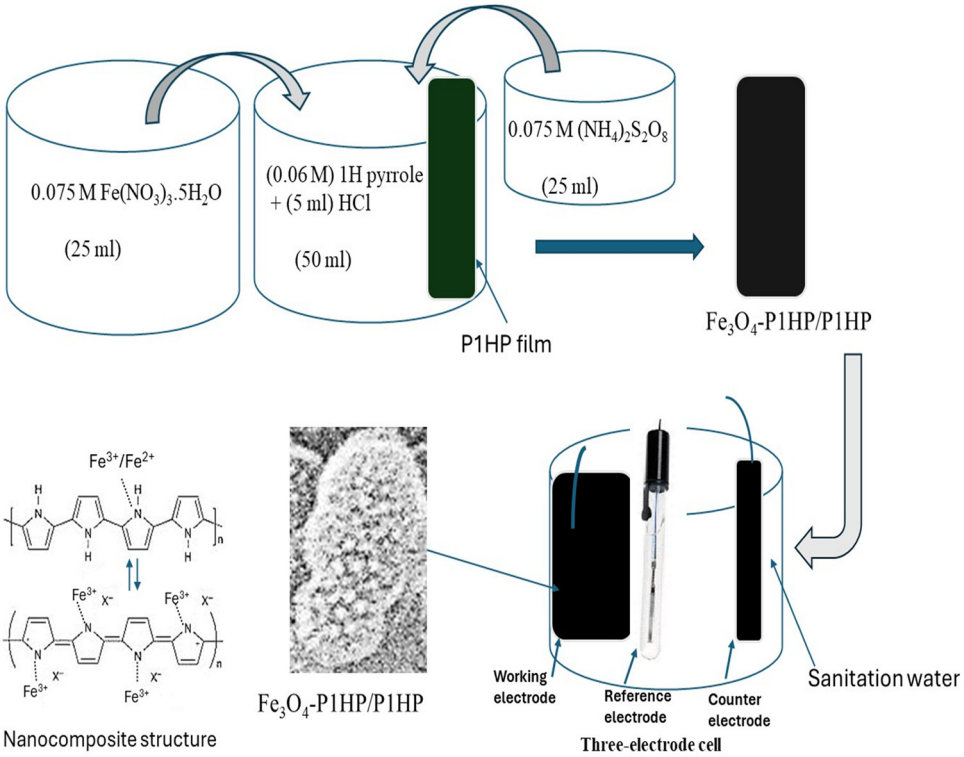

Figure 1: The fabrication and the applications of the Fe_3O_4-P1HP/P1HP photocathode inside a three-electrode cell for H_2 gas generation from sanitation water.

2.3 Photocathode for the hydrogen generation photoelectrochemically

Hydrogen generation is accomplished through the electrochemical splitting of sanitation water using a Fe_3O_4-P1HP/P1HP thin film deposited on a glass substrate. The process involves measuring the current density electrochemically with a CHI608E device, where the fabricated photocathode acts as the working electrode. Hydrogen production is evaluated via linear sweep voltammetry, comparing the generated J_{ph} to the initial J_o. The sanitation water used has a pH of 7.4, and its composition is detailed in Table 1. This method of converting environmentally harmful waste into hydrogen gas marks a significant advancement in waste-to-energy technology. The splitting reaction is conducted photoelectrochemically under a halide lamp (vacuum tube) that provides high-quality white light. The light can be filtered to generate specific monochromatic wavelengths, including 730, 540, 440, and 340 nm, by using various optical filters. These filters, circular and manufactured by Andover Corporation (model AM 106004, USA), allow only the desired wavelengths to pass through. The energy of the incident light is assessed in relation to the bandgap of the Fe_3O_4-P1HP/P1HP thin film photocathode. The hydrogen gas production is estimated by Faraday's law of electrolysis, as outlined in equation (1) [16]:

$$H_2\text{mole} = \int_0^t J_{ph} \cdot \frac{dt}{F}. \quad (1)$$

Table 1: Chemical constitution of the electrolyte (sanitation water) [17]

Material or element	Concentration (µg/l)
Ni^{3+}	0.01
F^-	0.001
Hg^{2+}	0.005
Mn^{2+}	0.001
Phenols	0.015
Ba^{3+}	0.002
NH_3	0.005
Cd^{3+}	0.05
Al^{3+}	0.003
As^{3+}	0.05
Cr^{3+}	0.001
Co^{2+}	0.002
Pb^{2+}	0.005
Zn^{2+}	0.005
Cu^{2+}	0.00015
Industrial washing	0.05
Fe^{3+}	0.0015
Coli groups	$4.0 \times 0.1\ cm^3$
Ag^+	0.01
Pesticides	0.02
CN^{-1}	0.01
Other cations	0.01

3 Results and discussion

3.1 Fe_3O_4-P1HP physicochemical characterization

The chemical characterization of Fe_3O_4-P1HP nanomaterials is conducted using various analytical tools, including FTIR spectroscopy, to identify the functional groups associated with the composite. The estimated vibration mode associated with the N–H group in P1HP is observed at 33,408 cm^{-1}, while the P1HP ring groups are identified at 1,551, 1,409, 1,313, 1,188, and 1,036 and 908 cm^{-1}, corresponding to the internal functional groups C–C, C═C, C–N, C–H, and out-of-plane bonds, respectively. The vibration modes of the composite show significant changes in P1HP upon the incorporation of Fe_3O_4. This incorporation substantially affects the bonds within the composite, altering both bond rotation and bond length. These alterations are evident through shifts in the positions of the bonds, as illustrated in Figure 2(a) and Table 2. The redshift observed in the bond positions indicates the impact of the Fe_3O_4 groups, with the bands associated with this oxide appearing at 789 and 625 cm^{-1}. These bands exhibit strong intensity compared to the pristine P1HP, highlighting the significant effect of Fe_3O_4 insertion on the composite structure.

The evaluation of the crystalline structure of the fabricated P1HP and Fe_3O_4/P1HP nanocomposite is illustrated in Figure 2(b). This analysis shows promising crystalline characteristics, particularly with regard to the peaks associated with Fe_3O_4, which are not present in the pristine P1HP due to its amorphous nature. The composite displays peaks at 16.7°, 29.6°, 34.9°, 36.1°, 41.4°, 56.4°, 54.8°, and 63.8°, corresponding to the growth directions of (111), (220), (311), (222), (400), (422), (511), and (440) planes, respectively [20]. These crystalline features indicate the successful incorporation of Fe_3O_4 into the composite.

The crystalline size of the nanocomposite is estimated using the Scherrer equation (equation (2)) [21,22], based on the peak observed at 2θ = 29.6°. The resulting crystalline size is calculated to be 53 nm. This fine crystalline size, combined with the favorable crystalline properties, suggests that the Fe_3O_4/P1HP nanocomposite is highly effective for optical applications. Specifically, the composite's ability to respond to light and utilize photon energy to generate hot electrons is particularly advantageous. These hot electrons can be

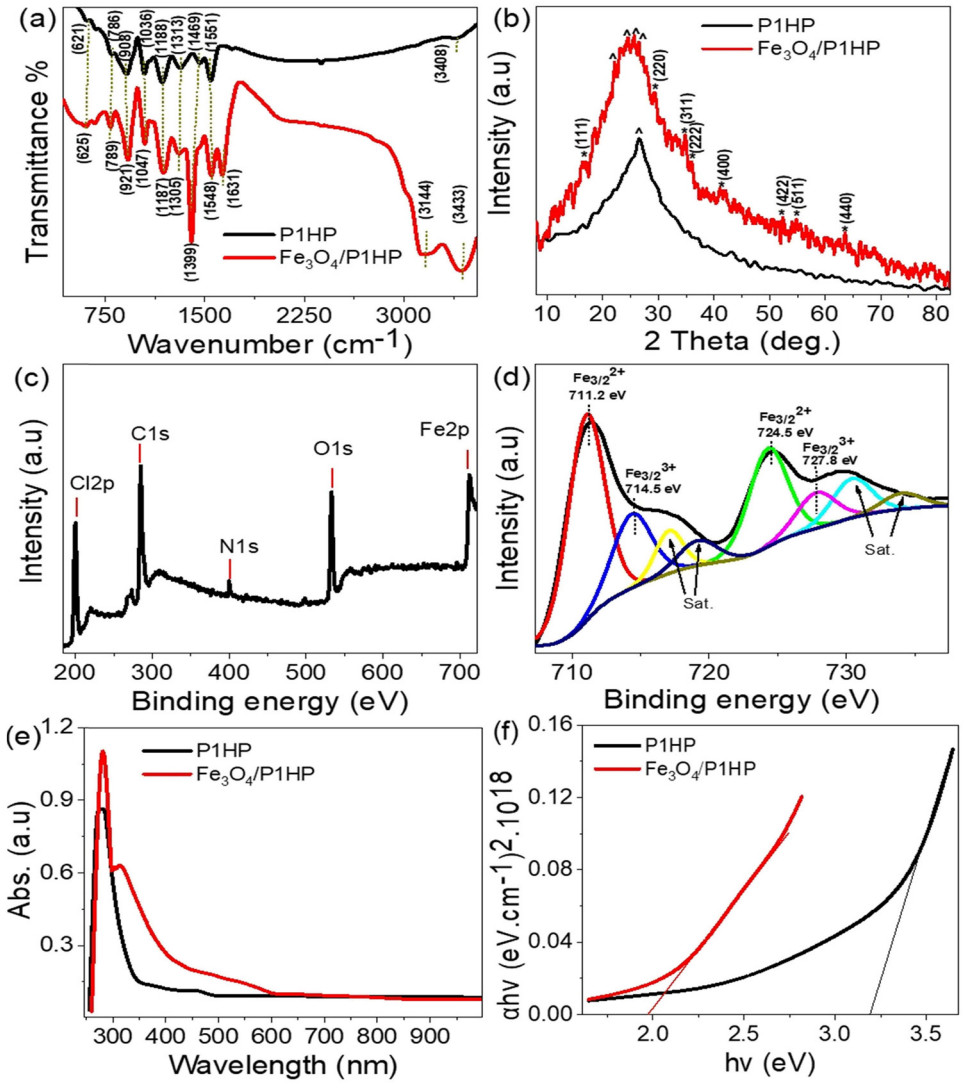

Figure 2: Chemical analyses of the Fe_3O_4-P1HP nanocomposite in comparison to P1HP: (a) FTIR, (b) XRD, (c) and (d) XPS survey, and Fe element, respectively. Optical analysis: (e) absorbance and (f) bandgap estimation.

harnessed for the generation of H_2 gas from wastewater, showcasing the composite's potential in energy conversion and environmental applications:

$$D = \frac{0.94\lambda}{\beta \cos\theta}. \quad (2)$$

To further emphasize the chemical characteristics of the fabricated Fe_3O_4/P1HP nanocomposite, XPS analyses are presented in Figure 2(c). These analyses illustrate the significant elemental oxidation behavior of both the organic and inorganic components within the composite. Specifically, the carbon and nitrogen elements are estimated at 285.2 and 401 eV, respectively. Oxygen (O), associated with the elements that form the inorganic structure through its connection with iron, is detected at 532 eV.

The XPS analysis also provides detailed information on the oxidation states of iron within the Fe_3O_4 material, highlighting the presence of both Fe^{2+} and Fe^{3+} states. This is

Table 2: Summary of estimated bonds from Figure 2(a) for the composite formation

Group and its value (cm^{-1})		Functional group
Fe_3O_4-P1HP	**P1HP**	
3,433	3,408	N–H [18]
1,631, 1,548, 1,399, 1,305, 1,187, 1,047, and 921	1,551, 1,409, 1,313, 1,188, 1,036, and 908	P1HP ring [19]
789 and 625	—	Fe–O

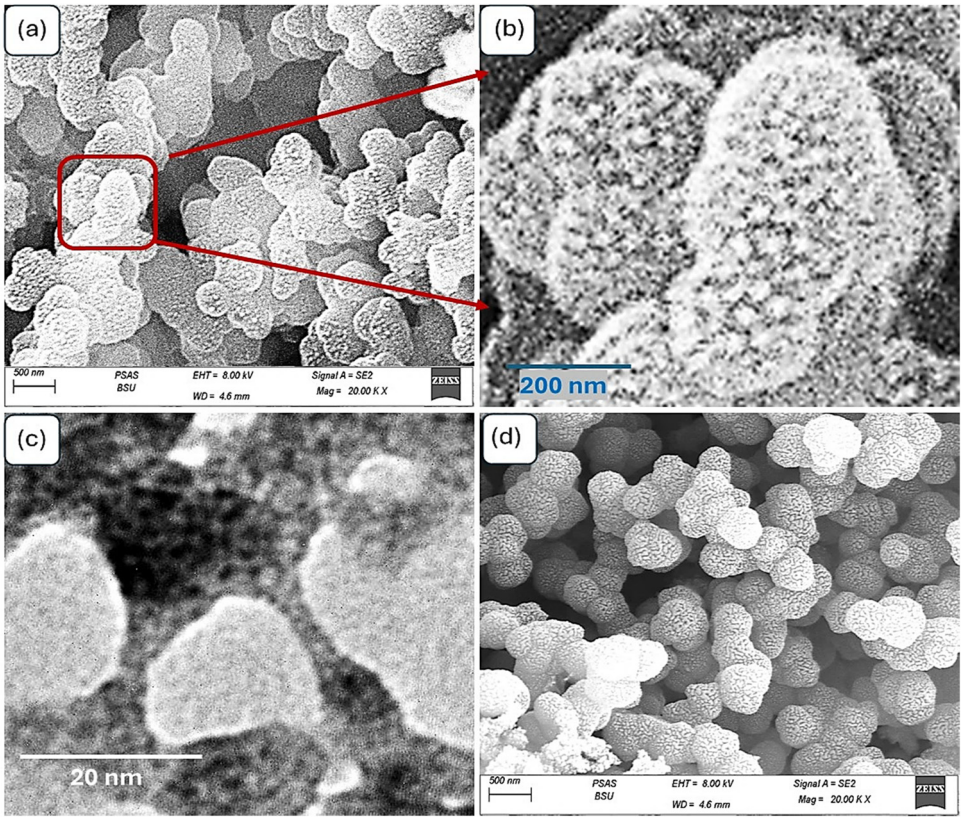

Figure 3: The morphological estimation of the Fe_3O_4-P1HP composite: (a) and (b) SEM at various magnifications, and (c) TEM. (d) SEM of the P1HP pristine polymer.

clearly shown in Figure 2(d), where the peaks corresponding to Fe^{2+} are identified at 711.2 and 724.5 eV for the $Fe2p_{3/2}$ and $Fe2p_{1/2}$ orbitals, respectively. In contrast, the peaks for Fe^{3+} are observed at slightly higher binding energies, with $Fe2p_{3/2}$ and $Fe2p_{1/2}$ orbitals at 714.5 and 727.8 eV, respectively [20]. The combination of these oxidation states confirms the formation of the Fe_3O_4 structure within the P1HP polymer network, contributing to the overall integrity and functionality of the Fe_3O_4/P1HP nanocomposite. This well-defined Fe_3O_4 structure embedded in the P1HP polymer is crucial for its enhanced optical properties. The nanocomposite exhibits significant photon absorption capabilities, making it highly effective for applications in renewable energy sources. The interaction of Fe_3O_4 with the P1HP matrix not only stabilizes the composite structure but also enhances its ability to harness photon energy efficiently. This property is particularly advantageous for generating hot electrons, for hydrogen production from wastewater.

The optical properties of the synthesized Fe_3O_4-P1HP nanocomposite, in comparison to P1HP, are depicted in Figure 2(e). The analysis shows significant changes in absorbance, marked by various peaks that reflect its responsiveness to incident photons. The Fe_3O_4-P1HP composite exhibits a broad absorbance spectrum extending up to 625 nm, reflecting its improved optical properties. Within this range, two distinct peaks are observed, corresponding to the two components of the composite: P1HP shows a UV peak, while Fe_3O_4 displays a visible peak. Beyond 625 nm, the composite's absorbance decreases, attributed to lower absorption values in the near-IR region. In contrast, P1HP exhibits an absorbance peak limited to 390 nm. Both materials share a common mechanism for these peaks, involving electron transfer and collection in the conduction band. However, the composite shows superior optical properties due to the larger absorbance regions, resulting in a higher quantity of collected electrons.

To highlight this difference, the bandgap values of both materials were estimated. The Fe_3O_4-P1HP composite has a bandgap of approximately 1.97 eV, whereas P1HP has a bandgap of 3.2 eV. These values were determined using the Tauc equation (equations (3) and (4)) [23,24], based on the absorbance coefficient (α):

$$\alpha h\nu = A(h\nu - E_g)^{1/2}, \tag{3}$$

$$\alpha = \left(\frac{2{,}303}{d}\right)A. \quad (4)$$

This comparison underscores the significant enhancement in the optical behavior of the Fe_3O_4-P1HP composite, making it more effective in photon absorption and related applications.

The synthesized Fe_3O_4-P1HP nanocomposite exhibits impressive morphology characterized by a highly porous nanostructure resembling a nano-cactus, as shown in Figure 3(a). This composite features excellent particle distribution, with porous regions between molecules contributing to its unique structure [25,26]. Each particle comprises numerous smaller internal particles, as depicted in Figure 3(b), which consist of nanofibers approximately 2.0 nm in length and porous structures around 5.0 nm. These porous structures aggregate to form a larger shape with an overall diameter of about 230 nm and a length of about 300 nm, resembling a nano-cactus. This morphology is advantageous for photon absorbance, as photons are trapped within the structure, allowing photon energy to be efficiently transferred to the particles. This process is conducive to the formation of hot electrons, which are then collected in the conducting band of the material [27,28].

This morphological feature is further confirmed through TEM analysis, as illustrated in Figure 3(c). The porous structure, evident in the TEM image, underscores the superior behavior of the Fe_3O_4-P1HP nanocomposite. The variation in color from faint to dark in the TEM images highlights the distinction between the organic P1HP and the inorganic Fe_3O_4 components, indicating a strong interface in the composite formation. The nanopores and nanoparticles are consistently around 5.0 nm in size.

Conversely, P1HP itself possesses notable features related to the formation of porous structured particles with a semi-circular shape. These particles exhibit unique porosity and size characteristics. This remarkable morphology contributes to the development of the Fe_3O_4-P1HP composite with its distinctive nano-cactus structure.

3.2 Fe_3O_4-P1HP/P1HP photocathode for the green hydrogen study

The study focuses on green hydrogen production through photoelectrochemistry, using a specially fabricated Fe_3O_4-P1HP/P1HP photocathode as the primary electrode within a three-electrode cell. This cell employs sanitation water as the electrolyte, with the aim of converting this water into green hydrogen gas. The use of sanitation water offers significant advantages due to its harmful nature and enrichment with heavy metals, which promote the electrolysis reaction necessary for H_2 gas formation. The process of H_2 gas generation occurs in several steps, beginning with the formation of OH radicals. These radicals attack additional H_2O molecules, facilitating the production of H_2 gas. The reaction is driven by hot electrons generated on the surface of the Fe_3O_4-P1HP/P1HP photocathode when exposed to light. These electrons are produced in high density and are subsequently transferred to H_2O via a reduction reaction.

The impact of light on the Fe_3O_4-P1HP/P1HP photocathode's performance is assessed through linear sweep voltammetry (Figure 4(a)) and chopped light measurements (Figure 4(b)). Figure 4(a) shows the effect of photon incidence in activating hot electrons from the Fe_3O_4-P1HP/P1HP surface, resulting in an increased production of H_2 gas. This is evidenced by the photocurrent density reaching −0.23 mA/cm², a significant improvement relative to the

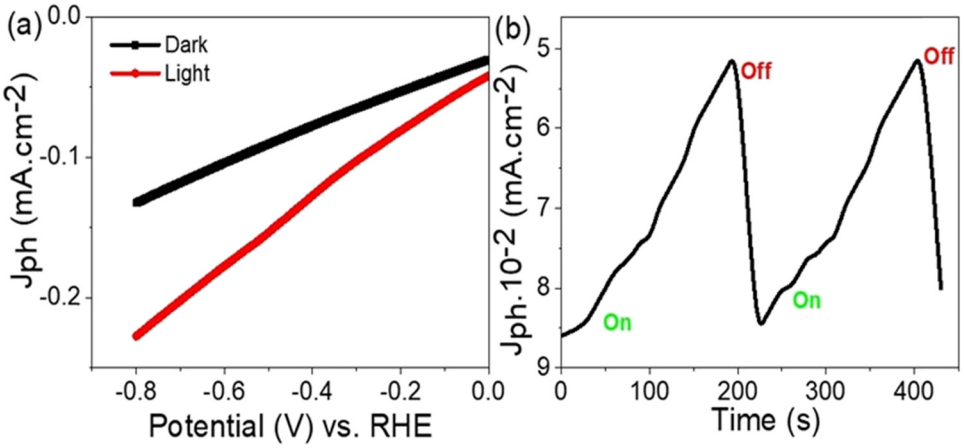

Figure 4: PEC testing of green H_2 gas production using the fabricated Fe_3O_4-P1HP/P1HP photocathode with wastewater as the electrolyte: (a) linear sweep voltammetry analysis showing the relationship between potential and current density, and (b) study under chopped light illumination.

J_o of −0.128 mA/cm². This indicates that photons greatly enhance the Fe_3O_4-P1HP/P1HP photocathode's efficiency, as both Fe_3O_4 and P1HP are photocatalytic materials enriched with hot electrons. These electrons are transferred from P1HP to Fe_3O_4, generating a strong electric field that initiates and drives the water-splitting reaction. The observed J_{ph} value highlights the promising potential of this approach for effectively splitting harmful sanitation water. Additionally, using sanitation water makes this a cost-effective process, especially when combined with the low-cost materials and techniques used, including the glass substrate for the thin-film deposition of the Fe_3O_4-P1HP/P1HP photocathode.

The sensitivity and reproducibility of the photocathode are further validated through the chopped light current measurements shown in Figure 4(b). The consistent J_{ph} and J_o relative to alternating light and dark conditions indicate the excellent stability of this photocathode. This stability is attributed to the P1HP material, which coats the Fe_3O_4 layer and acts as a protective barrier, enhancing the photocathode's resistance to corrosion. The overall results demonstrate that the Fe_3O_4-P1HP/P1HP photocathode not only achieves efficient hydrogen generation but also maintains high stability and reproducibility, making it a viable option for green hydrogen production from sanitation water.

The sensitivity of the fabricated Fe_3O_4-P1HP/P1HP photocathode was investigated by analyzing its response under varying light wavelengths and frequencies, achieved using a series of optical filters that selectively pass the desired wavelengths (as shown in Figure 5(a)). The study reveals that the photocurrent density increases with the photon energy, indicating a strong correlation between photon energy and the photocathode's performance [29–31]. The maximum J_{ph} values were observed at 340 and 440 nm, with corresponding values

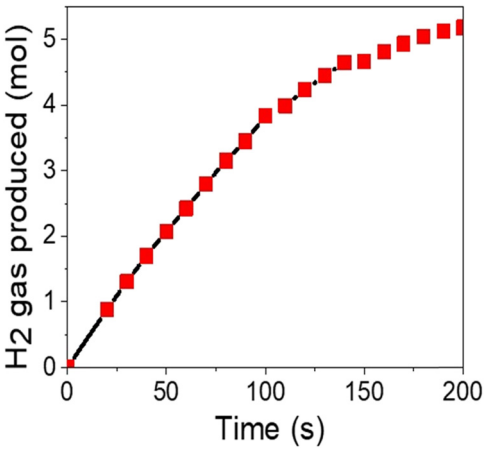

Figure 6: The estimated green H_2 produced moles using the fabricated Fe_3O_4-P1HP/P1HP photocathode with sanitation water as the electrolyte.

of −0.164 and −0.158 mA/cm², respectively. However, at 540 nm, the J_{ph} value decreased to −0.134 mA/cm² and reached its lowest point of −0.128 mA/cm² at 730 nm, a value that is essentially equivalent to J_o. This indicates that photons at 730 nm have no significant impact on the photocathode's performance.

The variation in J_{ph} values across different wavelengths highlights the photocathode's differing responsiveness to photons of various energies, underscoring the sensitivity of the fabricated Fe_3O_4-P1HP/P1HP photocathode. Figure 5(b) estimates the data obtained from the analysis, offering a clear comparison of the photocathode's response to different wavelengths.

To better understand the effect of photon energies on the fabricated photocathode, the photon energies at specific wavelengths (340, 440, and 540 nm) are compared with the

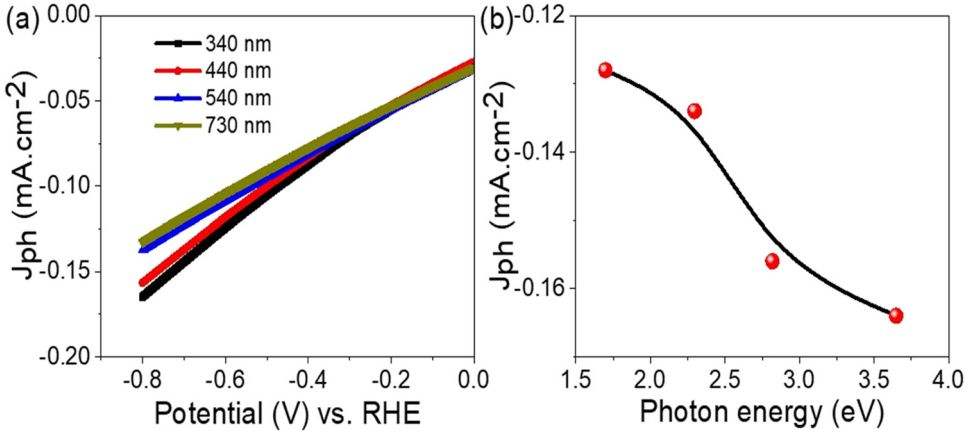

Figure 5: The influence of monochromatic light on the PEC testing of green H_2 gas production using the fabricated Fe_3O_4-P1HP/P1HP photocathode with wastewater as the electrolyte: (a) testing with optical filters at different wavelengths ranging from 340 to 730 nm, and (b) the resulting J_{ph} values under these various optical filters at −0.8 V.

Table 3: Comparison of the generated H_2 gas through the fabricated Fe_3O_4-P1HP/P1HP photocathode relative to other previous studies

Photoelectrode	J_{ph} (mA/cm^2)	Electrolyte
Polypyrrole/graphene oxide [33]	0.1	Sewage water
Polypyrrole/NiO [34]	0.11	Sewage water
Poly-3-methyl aniline/graphene oxide [35]	0.09	Sewage water
Cr_2S_3-Cr_2O_3/poly-2-aminobenzene-1-thiol [18]	0.017	Sewage water
Poly-O-aminothiophenol/intercalated iodide composite [16]	0.12	Red Sea water
Fe_3O_4-P1HP/P1HP (this work)	0.16	Sewage water

bandgap energy of the material, which is 1.97 eV. According to equation (5), the photon energies at 340, 440, and 540 nm are 3.6, 2.8, and 2.3 eV, respectively, all of which exceed the bandgap energy. As a result, these photons are capable of exciting electrons into the conduction band, causing the generation of hot electrons and a corresponding increase in the J_{ph} values.

However, the photon energy at 730 nm is 1.7 eV, which is lower than the bandgap energy. Because this energy is insufficient to promote electrons to the conduction band, it fails to generate hot electrons, resulting in a J_{ph} value that closely matches J_o. This lack of response at 730 nm further emphasizes the relationship between the photon energy and photocathode's ability to generate a photocurrent [31,32]:

$$E = hv. \tag{5}$$

The amount of H_2 gas generated was calculated using equation (1), as depicted in Figure 6. The results show a significant production of H_2 gas, measured at 0.09 mmol/cm^2 h. This impressive value highlights the potential of the fabricated Fe_3O_4-P1HP/P1HP photocathode for industrial applications in commercial hydrogen synthesis. In addition to the high yield, the photocathode offers technical advantages such as cost-effectiveness and the use of sanitation water as an electrolyte. These factors make the fabricated photocathode a promising and superior option relative to previous studies, as shown in Table 3.

4 Conclusions

The Fe_3O_4-P1HP/P1HP photocathode is constructed by the oxidation of pyrrole in the presence of $Fe(NO_3)_3$, which is carried out on a thin seeding film of P1HP. The resulting Fe_3O_4-P1HP composite features porous structures that cluster together, forming a larger configuration with an overall diameter of ~230 nm and a length of ~300 nm. This structure, with dendritic formations of about 2.0 nm on the surface, gives the composite a unique nano-cactus-like appearance.

The Fe_3O_4-P1HP/P1HP photocathode demonstrates strong performance in H_2 gas generation, as indicated by the photocurrent density (J_{ph}) measurements. Under light conditions, the J_{ph} value reaches −0.23 mA/cm^2. When exposed to monochromatic wavelengths, the photocathode achieves its highest J_{ph} values at 340 and 440 nm, recording −0.164 and −0.158 mA/cm^2, respectively. However, as the wavelength reaches 540 nm, the J_{ph} value declines to −0.134 mA/cm^2, eventually reaching its lowest point of −0.128 mA/cm^2 at 730 nm, which is comparable to J_o. This variation in J_{ph} values across different wavelengths reflects the photocathode's sensitivity to photon energies and its efficiency in generating hydrogen.

The fabricated photocathode exhibits a promising hydrogen generation rate of 90 μmol/h cm^2, showcasing its potential for industrial applications. The high hydrogen production rate, combined with the cost-effectiveness and ease of fabrication, indicates that this photocathode could be commercially viable for converting sanitation water into hydrogen gas. Its impressive performance, along with the economic and practical benefits, positions the Fe_3O_4-P1HP/P1HP photocathode as a strong contender for future large-scale H_2 production.

In summary, the Fe_3O_4-P1HP/P1HP photocathode offers a combination of efficient hydrogen generation and cost-effectiveness, making it a promising material for commercial applications. The unique structure and high performance under light conditions suggest that this technology could play a significant role in sustainable energy solutions, particularly in the conversion of sanitation water into hydrogen gas. With its potential for scalability and industrial use, the Fe_3O_4-P1HP/P1HP photocathode represents a valuable advancement in green hydrogen production.

Acknowledgments: Princess Nourah bint Abdulrahman University Researchers Supporting Project number (PNURSP2024R186), Princess Nourah bint Abdulrahman University, Riyadh, Saudi Arabia.

Funding information: This research was financially supported by Princess Nourah bint Abdulrahman University Researchers Supporting Project (number PNURSP2024R186),

Princess Nourah bint Abdulrahman University, Riyadh, Saudi Arabia.

Author contributions: Maha Abdallah Alnuwaiser: writing, funding, and ordering the work. Mohamed Rabia and Asmaa M Elsayed: conducting experiments and writing.

Conflict of interest: The authors have no conflict of interest.

Ethical approval: This study does not include any human or animal studies.

Data availability statement: All data generated or analyzed during this study are included in this article.

References

[1] Rabia M, Aldosari E, Geneidy AHA. Exceptionally crystalline nature of CrO3-Cr2O3/Ppy nanocomposite as a prospective photoelectrode for efficient green hydrogen generation in the context of environmentally friendly water-splitting reactions using sanitized water. Environ Prog Sustain Energy. 2024;43:e14455. doi: 10.1002/EP.14455.

[2] Giovanniello MA, Cybulsky AN, Schittekatte T, Mallapragada DS. The influence of additionality and time-matching requirements on the emissions from grid-connected hydrogen production. Nat Energy. 2024;2024:1–11. doi: 10.1038/s41560-023-01435-0.

[3] Constantinou P, Stock TJZ, Tseng L-T, Kazazis D, Muntwiler M, Vaz CAF, et al. EUV-induced hydrogen desorption as a step towards large-scale silicon quantum device patterning. Nat Commun. 2024;15:1–13. doi: 10.1038/s41467-024-44790-6.

[4] Tsao CW, Narra S, Kao JC, Lin YC, Chen CY, Chin YC, et al. Dual-plasmonic Au@Cu7S4 Yolk@shell nanocrystals for photocatalytic hydrogen production across visible to near infrared spectral region. Nat Commun. 2024;15:1–13. doi: 10.1038/s41467-023-44664-3.

[5] Purvis G, Šiller L, Crosskey A, Vincent J, Wills C, Sheriff J, et al. Generation of long-chain fatty acids by hydrogen-driven bicarbonate reduction in ancient alkaline hydrothermal vents. Commun Earth Environ. 2024;5:1–9. doi: 10.1038/s43247-023-01196-4.

[6] Barber J. Hydrogen derived from water as a sustainable solar fuel: Learning from biology. Sustain Energy Fuels. 2018;2:927–35.

[7] Wang M, Wan L, Luo J. Promoting CO_2 electroreduction on CuO nanowires with a hydrophobic nafion overlayer. Nanoscale. 2021;13:3588–93. doi: 10.1039/D0NR08369K.

[8] Zhang Y, Wan J, Zhang C, Cao X. MoS_2 and Fe_2O_3 Co-modify g-C3N4 to improve the performance of photocatalytic hydrogen production. Sci Rep. 2022;12:1–12. doi: 10.1038/s41598-022-07126-2.

[9] Momeni MM, Ghayeb Y, Mohammadi F. Solar water splitting for hydrogen production with Fe_2O_3 nanotubes prepared by anodizing method: Effect of anodizing time on performance of Fe_2O_3 nanotube arrays. J Mater Sci: Mater Electron. 2015;26:685–92. doi: 10.1007/S10854-014-2450-9/FIGURES/11.

[10] Alkallas FH, Ben Gouider Trabelsi A, Alrebdi TA, Ahmed AM, Rabia M. Development of a highly efficient optoelectronic device based on $CuFeO_2$/CuO/Cu composite nanomaterials. Materials. 2022;15:6857. doi: 10.3390/MA15196857.

[11] Lin YF, Chen JL, Xu CY, Chung TW. One-pot synthesis of paramagnetic iron(III) hydroxide nanoplates and ferrimagnetic magnetite nanoparticles for the removal of arsenic ions. Chem Eng J. 2014;250:409–15. doi: 10.1016/j.cej.2014.04.029.

[12] Elsayed AM, Rabia M, Shaban M, Aly AH, Ahmed AM. Preparation of hexagonal nanoporous Al_2O_3/TiO_2/TiN as a novel photodetector with high efficiency. Sci Rep. 2021;11:1–12. doi: 10.1038/s41598-021-96200-2.

[13] Blackwood D, Josowicz M. Work function and spectroscopic studies of interactions between conducting polymers and organic vapors. J Phys Chem. 1991;95:493–502. doi: 10.1021/J100154A086/ASSET/J100154A086.FP.PNG_V03.

[14] Rabia M, Mohamed HSH, Shaban M, Taha S. Preparation of polyaniline/PbS core-shell nano/microcomposite and its application for photocatalytic H2 electrogeneration from H_2O. Sci Rep. 2018;8:1–11. doi: 10.1038/s41598-018-19326-w.

[15] Shaban M, Rabia M, El-Sayed AMA, Ahmed A, Sayed S. Photocatalytic properties of PbS/graphene oxide/polyaniline electrode for hydrogen generation. Sci Rep. 2017;7:1–13. doi: 10.1038/s41598-017-14582-8.

[16] Rabia M, Aldosari E, Geneidy AHA. Highly flexible poly-*O*-aminothiophenol/intercalated iodide composite with highly morphological properties for green hydrogen generation from Red Sea water. Phys Scr. 2024;99:045001. doi: 10.1088/1402-4896/AD2BC5.

[17] Hadia NMA, Abdelazeez AAA, Alzaid M, Shaban M, Mohamed SH, Hoex B, et al. Converting sewage water into H2 fuel gas using Cu/CuO nanoporous photocatalytic electrodes. Materials. 2022;15:1489. doi: 10.3390/MA15041489.

[18] Rabia M, Elsayed AM, Alnuwaiser MA. Cr2S3-Cr2O3/poly-2-aminobenzene-1-thiol as a highly photocatalytic material for green hydrogen generation from sewage water. Micromachines. 2023;14:1567. doi: 10.3390/MI14081567.

[19] Sayyah SM, Shaban M, Rabia M. A high-sensitivity potentiometric mercuric ion sensor based on m-toluidine films. IEEE Sens J. 2016;16:1541–8. doi: 10.1109/JSEN.2015.2505313.

[20] Ai Q, Yuan Z, Huang R, Yang C, Jiang G, Xiong J, et al. One-pot co-precipitation synthesis of Fe_3O_4 nanoparticles embedded in 3D carbonaceous matrix as anode for lithium ion batteries. J Mater Sci. 2019;54:4212–24. doi: 10.1007/s10853-018-3141-3.

[21] Burton AW, Ong K, Rea T, Chan IY. On the estimation of average crystallite size of zeolites from the Scherrer equation: A critical evaluation of its application to zeolites with one-dimensional pore systems. Microporous Mesoporous Mater. 2009;117:75–90. doi: 10.1016/J.MICROMESO.2008.06.010.

[22] Lim DJ, Marks NA, Rowles MR. Universal Scherrer equation for graphene fragments. Carbon. 2020;162:475–80. doi: 10.1016/J.CARBON.2020.02.064.

[23] Haryński Ł, Olejnik A, Grochowska K, Siuzdak K. A facile method for tauc exponent and corresponding electronic transitions determination in semiconductors directly from UV–Vis spectroscopy data. Opt Mater. 2022;127:112205. doi: 10.1016/J.OPTMAT.2022.112205.

[24] Aziz SB, Nofal MM, Ghareeb HO, Dannoun EMA, Hussen SA, Hadi JM, et al. Characteristics of poly(vinyl alcohol) (PVA) based composites integrated with green synthesized Al3+-metal complex: Structural, optical, and localized density of state analysis. Polymers. 2021;13:1316. doi: 10.3390/POLYM13081316.

[25] Alnuwaiser MA, Rabia M. Hollow mushroom nanomaterials for potentiometric sensing of Pb 2+ ions in water via the intercalation of iodide ions into the polypyrrole matrix. Open Chemistry. 2024;22:20240217.
[26] Han T, Wei Y, Jin X, Jiu H, Zhang L, Sun Y, et al. Hydrothermal self-assembly of α-Fe_2O_3 nanorings@graphene aerogel composites for enhanced Li storage performance. J Mater Sci. 2019;54:7119–30. doi: 10.1007/S10853-019-03371-5/FIGURES/9.
[27] Kwon JH, Choi KC. Highly reliable and stretchable OLEDs based on facile patterning method: Toward stretchable organic optoelectronic devices. npj Flex Electron. 2024;8. doi: 10.1038/s41528-024-00303-5.
[28] Cai X, Suess RJ, Drew HD, Murphy TE, Yan J, Fuhrer MS. Pulsed near-IR photoresponse in a Bi-metal contacted graphene photodetector. Sci Rep. 2015;5:1–7. doi: 10.1038/srep14803.
[29] Jia Z, Qin S, Meng L, Ma Q, Angunawela I, Zhang J, et al. High performance tandem organic solar cells via a strongly infrared-absorbing narrow bandgap acceptor. Nat Commun. 2021;12:1–10. doi: 10.1038/s41467-020-20431-6.
[30] Rabia M, Shaban M, Adel A, Abdel-Khaliek AA. Effect of plasmonic Au nanoparticles on the photoactivity of polyaniline/indium tin oxide electrodes for water splitting. Environ Prog Sustain Energy. 2019;38:13171. doi: 10.1002/ep.13171.
[31] Ibrahim AM, Abdel-wahab MS, Elfayoumi MAK, Tawfik WZ. Highly efficient sputtered Ni-doped Cu_2O photoelectrodes for solar hydrogen generation from water-splitting. Int J Hydrogen Energy. 2023;48:1863–76. doi: 10.1016/J.IJHYDENE.2022.10.089.
[32] Chen Q-Y, Zhang K, Liu J-S, Wang Y-H. Hydrogen and electricity production in a light-assisted microbial photoelectrochemical cell with $CaFe_2O_4$ photocathode. J Photonics Energy. 2017;7:026501. doi: 10.1117/1.JPE.7.026501.
[33] Hamid MMA, Alruqi M, Elsayed AM, Atta MM, Hanafi HA, Rabia M. Testing the photo-electrocatalytic hydrogen production of polypyrrole quantum dot by combining with graphene oxide sheets on glass slide. J Mater Sci: Mater Electron. 2023;34:1–11. doi: 10.1007/S10854-023-10229-9/METRICS.
[34] Atta A, Negm H, Abdeltwab E, Rabia M, Abdelhamied MM. Facile fabrication of polypyrrole/NiOx core-shell nanocomposites for hydrogen production from wastewater. Polym Adv Technol. 2023;34(5):1633–41. doi: 10.1002/PAT.5997.
[35] Helmy A, Rabia M, Shaban M, Ashraf AM, Ahmed S, Ahmed AM. Graphite/rolled graphene oxide/carbon nanotube photoelectrode for water splitting of exhaust car solution. Int J Energy Res. 2020;44:7687–97. doi: 10.1002/er.5501.